Acta Pharmaceutica Sinica B 2023;13(1):315−326

Chinese Pharmaceutical Association
Institute of Materia Medica, Chinese Academy of Medical Sciences

Acta Pharmaceutica Sinica B

www.elsevier.com/locate/apsb
www.sciencedirect.com

ORIGINAL ARTICLE

Predatory bacterial hydrogels for topical treatment of infected wounds

Yan Liu[a,b], Bo Zhuang[c], Bochuan Yuan[b], Hui Zhang[b], Jingfei Li[b], Wanmei Wang[b], Ruiteng Li[b], Lina Du[b], Pingtian Ding[a], Yiguang Jin[a,b,*]

[a]*Department of Pharmaceutics, School of Pharmacy, Shenyang Pharmaceutical University, Shenyang 110016, China*
[b]*Department of Pharmaceutical Sciences, Beijing Institute of Radiation Medicine, Beijing 100850, China*
[c]*Department of Chemical Defense, Institute of NBC Defense, Beijing 102205, China*

Received 8 February 2022; received in revised form 22 April 2022; accepted 28 April 2022

KEY WORDS

Bacterial predator;
Bdellovibrio bacteriovorus;
Hydrogel;
Infected wound;
Polyvinyl alcohol;
Sodium alginate;
Vibrio vulnificus;
Wound healing

Abstract Wound infection is becoming a considerable healthcare crisis due to the abuse of antibiotics and the substantial production of multidrug-resistant bacteria. Seawater immersion wounds usually become a mortal trouble because of the infection of *Vibrio vulnificus*. *Bdellovibrio bacteriovorus*, one kind of natural predatory bacteria, is recognized as a promising biological therapy against intractable bacteria. Here, we prepared a *B. bacteriovorus*-loaded polyvinyl alcohol/alginate hydrogel for the topical treatment of the seawater immersion wounds infected by *V. vulnificus*. The *B. bacteriovorus*-loaded hydrogel (BG) owned highly microporous structures with the mean pore size of 90 μm, improving the rapid release of *B. bacteriovorus* from BG when contacting the aqueous surroundings. BG showed high biosafety with no L929 cell toxicity or hemolysis. More importantly, BG exhibited excellent *in vitro* anti-*V. vulnificus* effect. The highly effective infected wound treatment effect of BG was evaluated on mouse models, revealing significant reduction of local *V. vulnificus*, accelerated wound contraction, and alleviated inflammation. Besides the high bacterial inhibition of BG, BG remarkably reduced inflammatory response, promoted collagen deposition, neovascularization and re-epithelization, contributing to wound healing. BG is a promising topical biological formulation against infected wounds.

*Corresponding author. Tel.: +86 10 88215159.
E-mail address: jinyg@sina.com (Yiguang Jin).

Peer review under responsibility of Chinese Pharmaceutical Association and Institute of Materia Medica, Chinese Academy of Medical Sciences.

https://doi.org/10.1016/j.apsb.2022.05.005

1. Introduction

Wound infection caused by bacterial contamination is one of impediments for wound healing. Antibiotics are the most commonly used way to treat wound infections including *Vibrio vulnificus* induced wound infection in the hospital. However, due to the excessive use of antibiotics in human, agriculture, and aquaculture systems, antibiotic resistance has emerged and evolved in many bacteria including *V. vulnificus*[1]. Multidrug-resistant bacterial infections lead to a great amount of deaths, *e.g.*, approximately 23,000 deaths in 2 million infections in the United States every year[2]. One effective antibacterial way independent on the resistant mechanisms is urgently needed.

Seawater immersion (SWI) wounds are common in coastal regions and sea navigation, and usually infected with *V. vulnificus*[3]. *V. vulnificus* infected-SWI wounds are sometimes fatal because substantial sepsis takes place in susceptible individuals, also resulting in amputation[4,5]. The mortality rate of *V. vulnificus*-infected patients is up to nearly 20% and death may occur within one or two days after infection[6]. Early diagnosis, rational use of antibiotics, and timely debridement can save patients' lives[7]. Antibiotic treatment recommendations for *Vibrio* spp. infections include tetracyclines, fluoroquinolones, third-generation cephalosporins, aminoglycosides and folate pathway inhibitors[8]. Besides, some inorganic antibacterial agents such as silver, iodine and zinc oxide are also used for treatment of wound bacterial infection though their serious tissue toxicities are unavoidable[9]. It is urgent to develop safe and effective treatments of infected SWI wounds.

A predatory microorganism, *Bdellovibrio bacteriovorus*, attracts attention to possible achieve the above purpose. *B. bacteriovorus* is a small predatory bacterium that kills its preys including most Gram-negative bacteria (*e.g.*, *Escherichia coli*, *Pseudomonas aeruginosa*, *Acinetobacter baumannii*, *V. vulnificus*, etc.) and some Gram-positive bacteria (*e.g.*, *Staphylococcus aureus*) by entering the middle space between the wall and the out membrane of host bacteria to form bdelloplasts and multiplies[10]. Its unique action can be regarded as "parasitic" and "lytic"[11]. It is regarded as a replicable "live antibiotic", coevolving with bacteria[12]. It may become a potent weapon against drug-resistant bacteria[13–15]. More importantly, *B. bacteriovorus* is very safe for eukaryotic cells because it only acts on the microorganisms with the cell walls such as bacteria[16]. No apparent pathological effects or signs of cytotoxicity or reduction in cell viability are found when it contacts mammalian cells, including human cells and numerous animal models such as zebrafish, mice, rats, rabbits, guinea pigs, and chicks[13,17–20]. However, the growth and application of *B. bacteriovorus* depend on an appropriate environment that provides necessary preys, aqueous space, and air contact. In the previous studies, the environment is ignored so that the clinical application of *B. bacteriovorus* is limited. The topical application of *B. bacteriovorus* may become an opportunity, such as skin wound treatment.

Hydrogels are the crosslinking structure composed of hydrophilic polymers, water and other additives, which provides a proper environment for cell growth with necessary nutrition and oxygen supply[21]. The components of hydrogels include natural and synthetic polymers, such as chitosan, hyaluronic acid (HA), sodium alginate (SA), poly(ethylene glycol) (PEG), poly(lactic-*co*-glycolic acid) (PLGA), and poly(vinyl alcohol) (PVA), where PVA and SA are extensively used for delivery of living cells or microorganisms[22–24]. Hydrogels are an important wound dressing[25,26]. Many types of hydrogels have been applied for infectious skin wound healing *via* their antibacterial ability and the function of tissue regeneration scaffolds[27,28]. Recently, biodegradable interpenetrating polymer network dry cryogel hemostats, biomechanically active injectable self-healing hydrogels, and adhesive antioxidant antibacterial self-healing hydrogels present great potentials as novel wound dressings for rapid hemostasis and promoting wound healing[29–31].

Here, we designed a hydrogel formulation to load *B. bacteriovorus*, providing the appropriate environment for its growth and expanding its topical application in treatment of wound infection. The *B. bacteriovorus*-loaded PVA/SA hydrogel formulation was prepared for topical treatment of *V. vulnificus*-infected wounds. The hydrogel supplies a suitable environment for *B. bacteriovorus* survival and movement. The hydrogel combines the advantage of hydrogel-self for adherence and covering of wounds and the characteristic of highly effective antibacterial ability of *B. bacteriovorus* in spite of infectious bacterial types. We explored the preparation process, structures, biocompatibility and antimicrobial activity of the hydrogels. The improved wound healing and antibacterial mechanisms of the *B. bacteriovorus*-loaded hydrogel (BG) were investigated in details.

2. Materials and methods

2.1. Materials

Polyvinyl alcohol (PVA; MW 72,600−81,400 Da, 86%−90% hydrolyzed) was purchased from Shanghai Chenqi Chemical Tech. Co., Ltd. (Shanghai, China). Sodium alginate (SA; 200 ± 20 mPa s) was obtained from Beijing InnoChem Tech. Co., Ltd. (Beijing, China). A Luria−Bertani culture medium was purchased from Beijing Sanyao Technology Development Co., Ltd. (Beijing, China). Roswell Park Memorial Institute (RPMI 1640) culture media were provided by Invitrogen Life Tech. Co., Ltd. (California, USA). Fetal bovine serum (FBS) and trypsin-ethylene diamine tetraacetic acid (EDTA) were purchased from Gibco Life Technologies (CA, USA). Cell Counting Kit-8 (CCK-8) was purchased from Gen-view Scientific Inc. (NJ, USA). *V. vulnificus* (ATCC 27562) and *B. bacteriovorus* (ATCC 15356) were purchased from Biobw Biotechnology Co., Ltd. (Beijing, China). Fluorescein diacetate (FDA) and propidium iodide (PI) were purchased from Sinopharm Chemical Reagent Co., Ltd. (Shanghai, China). Other reagents were of analytic grade. Enzyme-linked immunosorbent assay (ELISA) kits of mouse IL-6 and TNF-α were purchased from Beijing Neobioscience Biochemical Tech. Co., Ltd. (Beijing, China). Aquacel® Ag (a silver-based dressing) was purchased from the ConvaTec company (Princeton, USA). SYBR qPCR Master Mix and Taq Master Mix were purchased from Vazyme Biotech Co., Ltd. (Nanjing, China).

2.2. Cells and animals

A normal murine fibroblast L929 cell line was purchased from the Cell Bank of the Chinese Academy of Sciences (Shanghai, China) and cultured in the RPMI 1640 supplemented with 10% FBS at 37 °C in a humidified 5% CO_2 atmosphere.

Male ICR mice (18−20 g) were purchased from the SPF Biotechnology Co., Ltd. (Beijing, China). Mice were housed under the constant conditions of humidity (50 ± 5%) and temperature (25 ± 1 °C) with 12−12 h light−dark cycles. Food and

water were available ad libitum. All experimental procedures were approved by the Animal Care and Use Committee of Beijing Institute of Radiation Medicine and complied with the principles of laboratory animal care and use guidelines.

2.3. Preparation of BG

PVA/SA hydrogels were prepared referred to the literature with modifications[32,33]. Briefly, an aqueous solution of 10% PVA and 4% SA was prepared and transferred to a Petri dish followed by freeze-thawing with 5 cycles (−20 °C for 20 h and room temperature for 4 h) until PVA full crosslinking to form a hydrogel. The hydrogel was immersed in a $CaCl_2$ (0.1 mol/L) solution for 3 h to make SA complete crosslinking. The hydrogel was washed with water several times and then freeze-dried in a lyophilizer (LGJ-30F, Songyuan Huaxing Technology Develop Co., Ltd., China) to obtain dried hydrogels. A *B. bacteriovorus* (8×10^8 PFU/mL) suspension (0.2 mL) was added to the dried hydrogel (0.01 g, 10 mm in diameter) to obtain BG before application to wounds. Single BG discs containing 10^8 *B. bacteriovorus* owned the similar antibacterial efficiency to single BG discs containing 10^9 *B. bacteriovorus* (Supporting Information Fig. S1). Therefore, we selected single BG discs containing 10^8 *B. bacteriovorus* in the following exploration. Meanwhile, a blank hydrogel was obtained after a dried hydrogel swelled in saline.

2.4. Observation of B. bacteriovorus and BG

The morphology of *B. bacteriovorus* was observed under a transmission electron microscope (TEM, HITACHI H-7650, 80 kV, Japan). One drop (5 μL) of *B. bacteriovorus* suspensions was placed on a microscopic copper grid and the excess liquid was removed using filter paper. The sample was then negatively stained with a 5% phosphotungstic acid solution (pH 7.0) for 3 min and air-dried followed by observation under the TEM. In addition, one drop (5 μL) of the suspension containing *B. bacteriovorus* and *V. vulnificus* was also placed on a microscopic copper grid and then processed as above.

The morphology of BG was investigated under a scanning electron microscope (SEM, EmCrafts CUBE II, 20 kV, Korea). Briefly, the freshly prepared BG was instantly frozen with liquid nitrogen to maintain the inner structure of hydrogels and lyophilized. The freeze-dried BG was sliced up carefully. The section was sputter-coated with gold and observed under the SEM.

2.5. Cytotoxicity test

Cytotoxicity of formulations was evaluated in direct contact manner. L929 cells were directly covered with materials and then assayed using the Live/Dead staining method[34]. L929 cells (1×10^5 cells/well) were seeded in a 6-well plate with coverslips at the bottoms and incubated for 12 h. *B. bacteriovorus*, blank hydrogels, BG and Aquacel Ag were directly added to the cells, respectively, and incubated for 24 h at 37 °C. The materials and culture media were discarded and the cells were washed with phosphate buffered solutions (PBS) for several times. The cells were stained with the mixed solution of FDA (5 μg/mL) and PI (5 μg/mL) for 5 min and then thoroughly washed with PBS. The coverslips were withdrawn, put on glass slides, and inspected under a Nikon Eclipse Ti fluorescent microscope (Tokyo, Japan).

Cytotoxicity of formulations was further evaluated with the CCK-8 assay. L929 cells (5×10^3 cells/well) were seeded in 96-well plates and incubated overnight for adhesion. Extracts of blank hydrogels, BG and Aquacel Ag were prepared by immersing them in the cell culture media for 24 h at 37 °C. The cells were co-incubated with the above extracts and the media containing *B. bacteriovorus* for 24 h. The culture media were replaced with 100 μL of 10% CCK-8 reagents. After incubation for 2 h at 37 °C, the optical density (OD) was measured at 450 nm using a Biotek ELx800 plate reader (Biotek Instruments, Winooski, VT, USA). Cell viabilities were calculated as Eq. (1):

$$\text{Cell viability (\%)} = (OD_{sample} - OD_{blank})/(OD_{control} - OD_{blank}) \times 100 \quad (1)$$

2.6. Hemolysis assay

Hemolysis assays of formulations were conducted with mouse's red blood cells (RBCs) referred to the literature[35]. Briefly, 2% RBC suspensions were mixed with *B. bacteriovorus*, blank hydrogels, BG, Aquacel Ag, saline (negative control), and 1% Triton X-100 solutions (positive control) at 37 °C for 4 h, respectively. After the suspensions were centrifuged at 2000 rpm and 4 °C for 10 min (H2-16 KR, Hunan Kecheng Instrument and Equipment Co., Ltd., Changsha, China), the OD of supernatants was measured with a UV−Vis spectrophotometer (TU-1901, Beijing Purkinje General Instrument Co., Ltd., Beijing, China) at 540 nm. Hemolysis rates were calculated as Eq. (2):

$$\text{Hemolysis rate (\%)} = (OD_{sample} - OD_{negative})/(OD_{positive} - OD_{negative}) \times 100 \quad (2)$$

2.7. Lysis kinetics of B. bacteriovorus against V. vulnificus

A *V. vulnificus* suspension (1×10^8 CFU/mL, 150 μL/well) and a *B. bacteriovorus* suspension (1×10^6 PFU/mL, 50 μL/well) were mixed and transferred to 96-well plates. A *B. bacteriovorus*-free suspension supplemented with diluted nutrient broth was used as the control. The plate was incubated on a rotary shaker at 200 rpm and 37 °C. OD values were examined at 600 nm at the predetermined time (12, 16, 20, 24, 30, 48, 60, and 72 h) with the microplate reader (Spark, Tecan Group Ltd., Switzerland). The kinetic lysis curve of *V. vulnificus* by *B. bacteriovorus* was plotted against the OD values.

2.8. qPCR determination of B. bacteriovorus copy numbers

Five primers were designed from the unique conserved region of *B. bacteriovorus* based on the alignment of the 16S rDNA sequences available in GenBank, including 94F, TCTGTCAGATGGGAAGAATGGTC; 113F, GGTCATTGGTCTAATAGGCCTT; 306R, ATAGTTTCAGACGCAGTTTCGG; 310R, ATTGATAGTTTCAGACGCAGTTTCGG; 336R, TTCCACTTCCCCCTCCAAC. Six primer pairs were paired for the next amplification investigation and the optimal pair of primers was selected by PCR (polymerase chain reaction) electrophoresis analysis. The standard curve method was used for the quantification of *B. bacteriovorus* solutions with serial dilutions of *B. bacteriovorus*. An aliquot (20 μL) reaction solution in the specific qPCR (quantitative PCR) assay contained 10 μL of SYBR qPCR Master Mix (Vazyme), 0.4 μL of each primer (10 μmol/L), 1 μL of template and 8.2 μL of ddH_2O. The PCR procedure included 95 °C for 3 min, 40 cycles

of 95 °C for 10 s, 60 °C for 10 s, 72 °C for 30 s, 95 °C for 15 s, 60 °C for 60 s, and 95 °C for 15 s in turn. All experiments were performed in triplicate.

2.9. *In vitro release of B. bacteriovorus from BG*

A BG disc (10 mm in diameter) was added to 900 μL of sterile water followed by gentle shaking (80 rpm) at 34 °C. An aliquot (10 μL) of release media was withdrawn at the predetermined time points (0, 0.167, 0.5, 1, 2, 4, 8, and 24 h) and the released *B. bacteriovorus* was determined with the above qPCR method.

2.10. *Antibacterial experiment*

The antibacterial ability of BG against *V. vulnificus* was evaluated with the inhibition zone method. A *V. vulnificus* suspension (1×10^8 CFU/mL, 100 μL) in LB media was evenly spread on the agar surface of a plate. A saline-immersed sterile paper disc, a blank hydrogel disc, an Aquacel Ag disc and a BG disc were placed on the agar surface of the single plate, respectively. All the discs had the diameter of 10 mm and the three plates were employed. The plates were preserved in an incubator for 24 h at 37 °C. Inhibition zones were measured with a digital vernier caliper and photographed. Moreover, a series of fresh BG were preserved at 4 °C for 1, 3, 5, and 7 days, respectively, and their antibacterial ability was also investigated as above.

2.11. *Treatment of V. vulnificus-infected wounds*

V. vulnificus-infected skin wounds were prepared as follows. The mice were anesthetized with 4% chloral hydrate solutions. The dorsal hair of mice was shaved and a circular (10 mm in diameter) of full-thickness skins was cut off to obtain a full-thickness skin wound. The wound was covered with a seawater-soaked sterile gauze for 1 h to mimic SWI and then infected by dropping a *V. vulnificus* suspension (1×10^7 CFU in 50 μL PBS) on the wound. Fifty-four mice were injured and infected. They were randomly divided into three groups (18 mice/group), including the infected control group without treatment, the Aquacel Ag treatment group, and the BG treatment group. The wounds in the two treatment groups were covered with Aquacel Ag and BG discs of 10 mm in diameter, respectively. The wounds in the infected control group were only covered with sterile gauzes. In addition, the full-thickness skins of 18 mice were cut off and they were as the uninfected control group without infection, in which the wounds were only covered with sterile gauzes. All the used formulations were fixed with medical bandages. Both Aquacel Ag and BG were refreshed on Days 3 and 7. The wounds were photographed on Days 0, 3, 7, and 10, and the wound area was analyzed using ImageJ software (the National Institute of Health, USA). Wound recovery rates were calculated as Eq. (3):

$$\text{Wound recovery rate } (\%) = (A_0 - A_t)/A_0 \times 100 \quad (3)$$

A_0 represents the wound area on Day 0, and A_t indicates the wound area at measuring time points.

Six mice each group were sacrificed on Days 3, 7, and 10, respectively, and the wound tissues were excised. The skin samples of three mice each group were used to determine inflammatory cytokines, and the other samples were used in histopathological and immunohistochemical studies.

2.12. *Determination of bacteria and inflammatory cytokines in wounds*

Exudate (2 μL) was collected from the wounds of three mice in the infected control group, the Aquacel Ag group, and the BG group on Day 3, respectively. The exudate was 100 times diluted with PBS. The dilution (50 μL) was evenly spread on nutrient agar plates. Bacterial colonies were counted after cultivation for 24 h at 37 °C.

The excised wound samples of three mice each group were homogenized with sterile saline to get 10% (*w*/*v*) homogenates. The wound homogenates were centrifuged at 5000×*g*, 4 °C for 15 min (Kecheng Instrument and Equipment Co., Ltd.). The supernatants were collected to determine the inflammatory cytokines (TNF-α and IL-6) with the enzyme-linked immunosorbent assay (ELISA) kits. OD values at 450 nm were determined with the microplate reader (Biotek Instruments), which were used to calculate the cytokine concentrations.

2.13. *Histopathology and immunohistochemistry*

The excised wound tissues of three mice each group were fixed in 4% (*w*/*v*) paraformaldehyde buffers, dehydrated with ethanol, and placed in xylene. The samples were embedded in paraffin, cut into ultrathin sections, and separately stained with hematoxylin-eosin (H&E) and Masson's trichrome. The stained samples were photographed with a microscope (BDS200-FL, Chongqing Optec Instrument Co., Ltd., Chongqing, China) to inspect histological changes.

The sample sections for immunohistochemical staining were incubated with 5% BSA at room temperature for 30 min to block nonspecific binding sites. The slices were washed with PBS and separately incubated with the primary antibodies anti-CD31 and F4/80 (Abcam, 1:200 dilution) at 4 °C overnight. The samples were washed with PBS, and incubated with the secondary antibodies that were HRP-labelled goat anti-rabbit IgG (Abcam, 1:200 dilution) for 50 min at room temperature. A DAB kit was applied for color developing and then the nuclei were stained with hematoxylin. The samples were dehydrated with ethanol, mounted with neutral resin, and photographed with the microscope (Chongqing Optec Instrument Co., Ltd.). Expression levels of CD31 and F4/80 were quantified by Image-Pro Plus software (Media Cybernetics, Inc., USA).

2.14. *Statistical analysis*

All data expressing as mean ± standard deviation (SD) of at least three replicates were analyzed statistically using SPSS 16.0 software (SPSS, Chicago, IL, USA). One-way analysis of variance (ANOVA) with the LSD test was carried out to compare between multiple groups. Statistical difference was considered to be significant when $P < 0.05$.

3. Results and discussion

3.1. *Characteristics of B. bacteriovorus and BG*

B. bacteriovorus was a tiny, motile, delta-proteobacteria of about 0.4 × 1.4 μm in size with a long polar flagellum (Fig. 1A). The strong swimming ability of *B. bacteriovorus* allowed it approaching its prey. We observed that *B. bacteriovorus* were

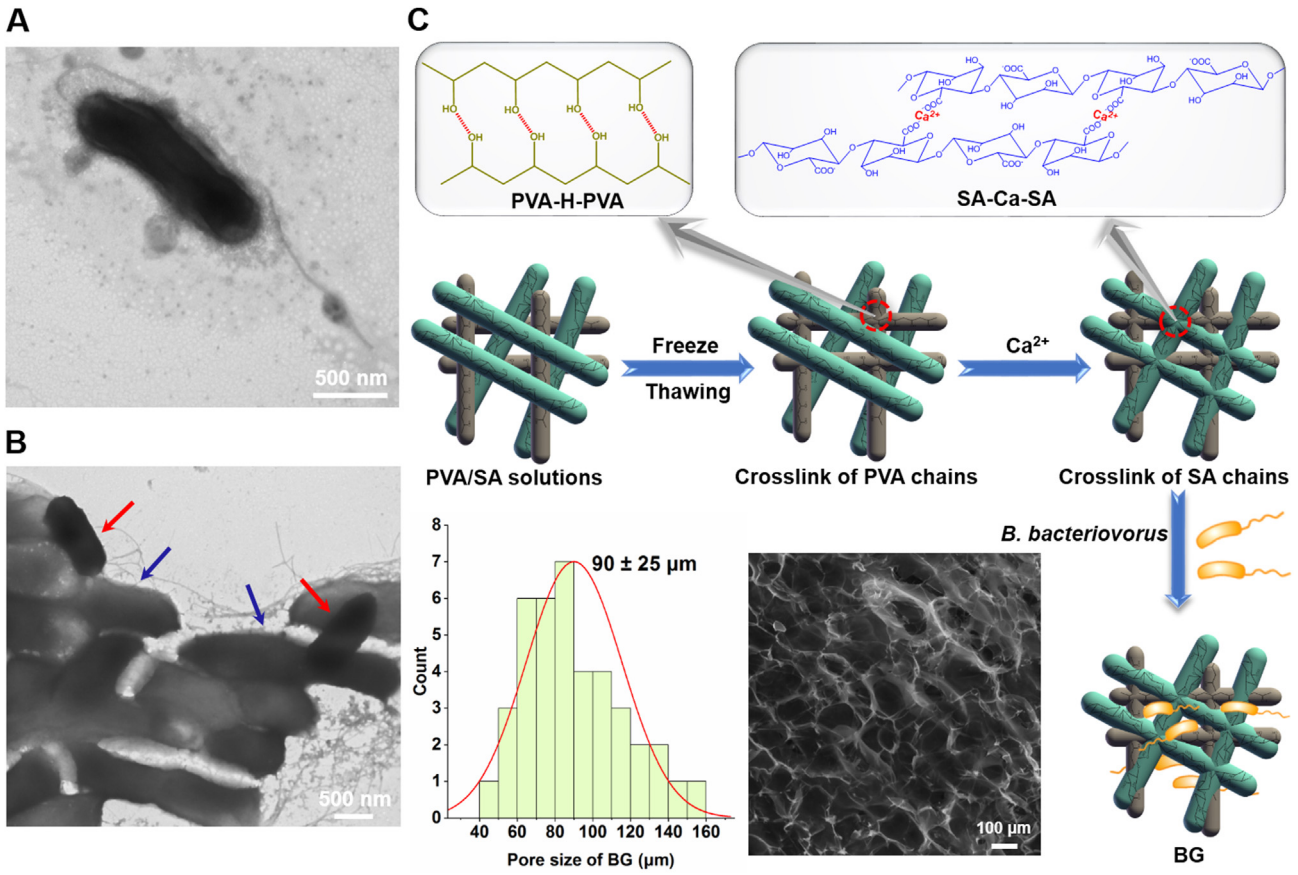

Figure 1 Characteristics of *B. bacteriovorus* and BG. TEM images of single *B. bacteriovorus* (A), and *B. bacteriovorus* (indicated with red arrows) invading *V. vulnificus* (indicated with blue arrows) (B). Preparation procedure of BG and its SEM image and its pore size distribution (C).

significantly attacking its prey (*i.e.*, *V. vulnificus*) by attaching the bacterial surface and penetrating the cell wall (Fig. 1B). It would multiply inside the host cells and cause the lysis of infested cells. Many progeny *B. bacteriovorus* would release from the destroyed prey and invade the next prey and this phenomenon was also reported by others[18,36].

The freeze-dried BG was highly porous like homogenous sponges (Fig. 1C). The mean pore size was 90 ± 25 μm according to the analysis of ImageJ software (Fig. 1C). The porous structure of hydrogels can well absorb wound exudates and maintain a proper humid condition. In addition, the porous hydrogel would make *B. bacteriovorus* free swimming and nutrients and oxygen transferring, favoring *B. bacteriovorus* approaching and capturing the prey.

The unique porous structure of the hydrogel was formed based on the interpenetrating network of PVA/SA, which resulted from freeze-thawing-induced crosslinking of PVA and Ca^{2+}-induced crosslinking of SA (Fig. 1C). PVA can be physically cross-linked without any crosslinking agents[37]. Whereas, SA changes to gels only after Na^{+} is replaced by divalent cations, such as Ca^{2+}, Ba^{2+} and Zn^{2+}, forming the egg-box structure[38]. SA hydrogels are the good scaffold for tissue engineering, guiding and promoting cell adhesion, growth, even the formation of new tissues based on their similar structure to the natural extracellular matrix[39]. However, only single PVA or SA hydrogels are not optimal for wound healing because of the low stability of SA hydrogels and the weak cell attachment of PVA hydrogels[40,41]. In this study, we prepared the dual-network PVA/SA hydrogel to achieve the tissue adhesion, improve wound healing, and load *B. bacteriovorus*. In addition, the temporary preparation of BG before application from the lyophilized PVA/SA hydrogel and *B. bacteriovorus* suspensions can ensure the quality of hydrogels and the activity of *B. bacteriovorus*.

3.2. *High safety of BG*

The cell safety of materials for wound healing is important because they directly contact the epidermal tissues and even enter the body[42]. We found that *B. bacteriovorus*, blank hydrogels and BG showed high L929 cell cytocompatibility according to the Live/Dead staining assay results with high cell viability after 24 h co-incubation, where the cells still maintained the same normal spindle shape as the control (Fig. 2A). Other reports also demonstrate the biosafety of *B. bacteriovorus* because it cannot interact with eukaryotic cells[43]. The biosafety of PVA and SA is also confirmed in wound healing treatment[44]. By contrast, Aquacel Ag remarkably induced the death of L929 cells (Fig. 2A). Only less than 50% cell viability was shown for the 50% extract of Aquacel Ag, and in the case of the 100% extract of Aquacel Ag, the cell viability decreased to about 40% (Fig. 2B). Ag^{+} ions interact with proteins to exhibit bacterial toxicity and they also lead to the toxic effect on cells due to its intrinsic property[45].

Hemolysis experiments further demonstrated the biosafety of *B. bacteriovorus*, blank hydrogels and BG, and moreover, the toxicity of Aquacel Ag. The supernatants were nearly colorless

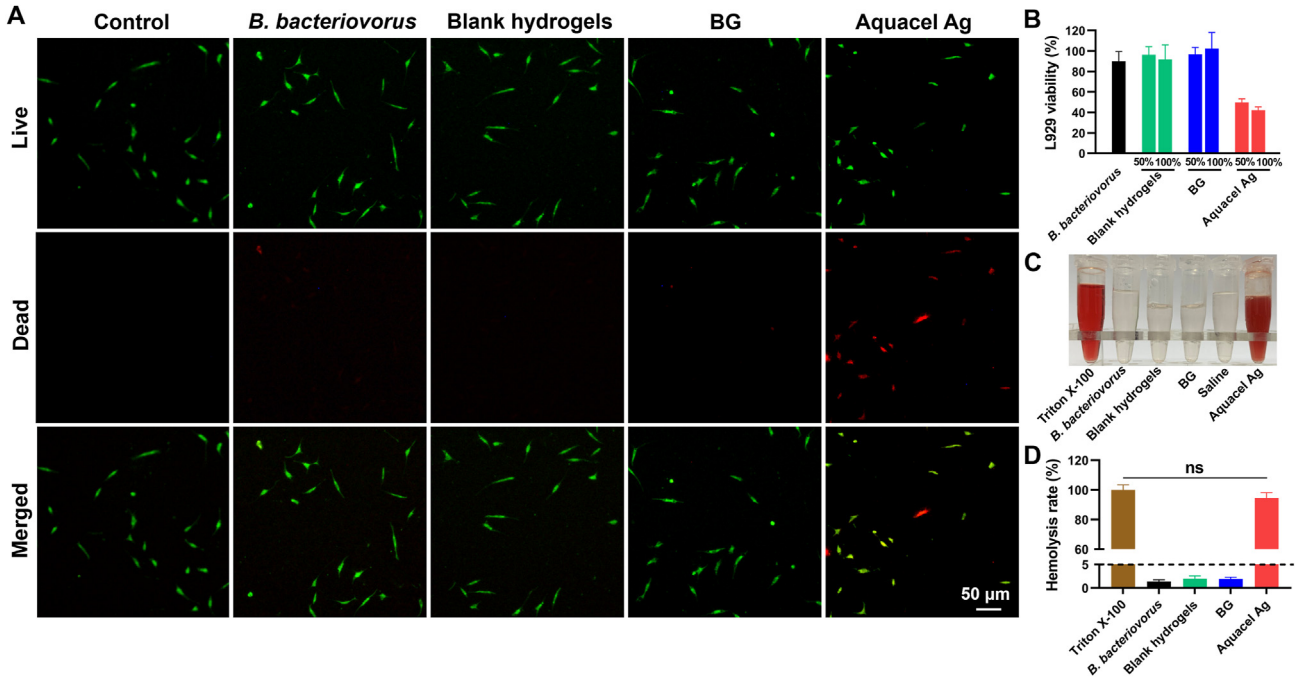

Figure 2 *In vitro* biocompatibility of *B. bacteriovorus*, blank hydrogels, BG, and Aquacel Ag. (A) Live/dead staining images of L929 cells in different groups. (B) L929 cell viability after co-incubation with *B. bacteriovorus*, the extracts of blank hydrogels, BG, and Aquacel Ag. (C) Photographs of the supernatants after RBC co-incubation with Triton X-100 (positive control), *B. bacteriovorus*, blank hydrogels, BG, saline (negative control), and Aquacel Ag. (D) Hemolysis rates of different samples. Data are presented as mean ± SD ($n = 3$; ns, not significant).

and transparent after co-incubation of RBC suspensions and the above materials with the very low hemolysis rates of less than 2% (Fig. 2C and D), indicating no hemolysis. In contrast, Aquacel Ag induced serious hemolysis with the similar red supernatants and the hemolysis rate (about 94%) to Triton X-100 (Fig. 2C and D). Other reports also showed the hemolysis of Ag^+ formulations[46]. Therefore, the high safety of BG would make it more suitable as the treatment of infected wounds than Aquacel Ag.

B. bacteriovorus is non-toxic and non-pathogenic when delivered *via* inhalation, oral, eye or directly injected into animals[17,47,48]. *B. bacteriovorus* has the unique lipopolysaccharide (LPS) that owns a neutral lipid A different from the negatively charged phosphate residues in the LPS of pathogenic bacteria[49]. It is known that the negatively charged LPS is the major reason of serious inflammatory response. Aquacel Ag is clinically applied based on its strong bacteria-killing ability; however, it also exhibits cytotoxicity to mammalian cells[50], often resulting in delayed wound re-epithelialization[51,52]. *B. bacteriovorus* is definitely scavenged and removed by the immune cells in the body so that *B. bacteriovorus* is safe[13,17–20]. However, this feature limits its application in the deep tissues. In this study, we used the *B. bacteriovorus* hydrogel formulation topically in the surface wounds that had much fewer immune cells than the deep tissues, which provided the opportunity to apply *B. bacteriovorus* formulations. Moreover, if a little *B. bacteriovorus* could enter the deep tissues, they would be quickly removed by the immune system.

3.3. *Rapid release of B. bacteriovorus from BG*

The pair of primers (113F and 306R) was optimal in the PCR electrophoresis analysis of *B. bacteriovorus* based on its highest PCR amplification efficiency and no primer dimer (Supporting Information Fig. S2). A linear standard curve was obtained in the range of 10^1–10^6 *B. bacteriovorus* copies per reaction. The bacterial copy numbers in the solutions were calculated by the linear equation based on C_t values (Fig. 3A). After BG contacted the sterile water, *B. bacteriovorus* quickly released to the surroundings to achieve 2.67×10^7 PFU/mL, and the rapid release profile maintained within 2 h (Fig. 3B), which was beneficial to its antibacterial effect. The rapid and complete release behavior of *B. bacteriovorus* from BG may be related to the good motility of *B. bacteriovorus* and the porous structure of the PVA/SA hydrogel (Fig. 1).

3.4. *High bactericidal ability of BG*

B. bacteriovorus is a highly motile Gram-negative predatory bacterium, possessing the ability to control a variety of pathogen infections *in vitro*[18,53]. *V. vulnificus* alone rapidly grew within 24 h with developing opacification and accelerating OD_{600} values followed by slow decreasing profiles due to space limitations (Fig. 4A). In contrast, the mixture of *B. bacteriovorus* and *V. vulnificus* maintained transparent and always showed decreasing OD_{600} profiles, indicating the gradual disappearance of *V. vulnificus* (Fig. 4A). Therefore, *B. bacteriovorus* had strong inhibition ability on the growth of *V. vulnificus*.

The strong bacterial inhibition ability of *B. bacteriovorus* was also demonstrated by the inhibition zone assay. In one plate, *B. bacteriovorus* showed a much larger inhibition zone against *V. vulnificus* than Aquacel Ag while saline and blank hydrogels had no inhibition zone (Fig. 4B). Moreover, the inhibition zone diameter (24.5 ± 0.7 mm) of BG had very significant difference ($P < 0.001$) from that (14.6 ± 0.7 mm) of Aquacel Ag (Fig. 4C).

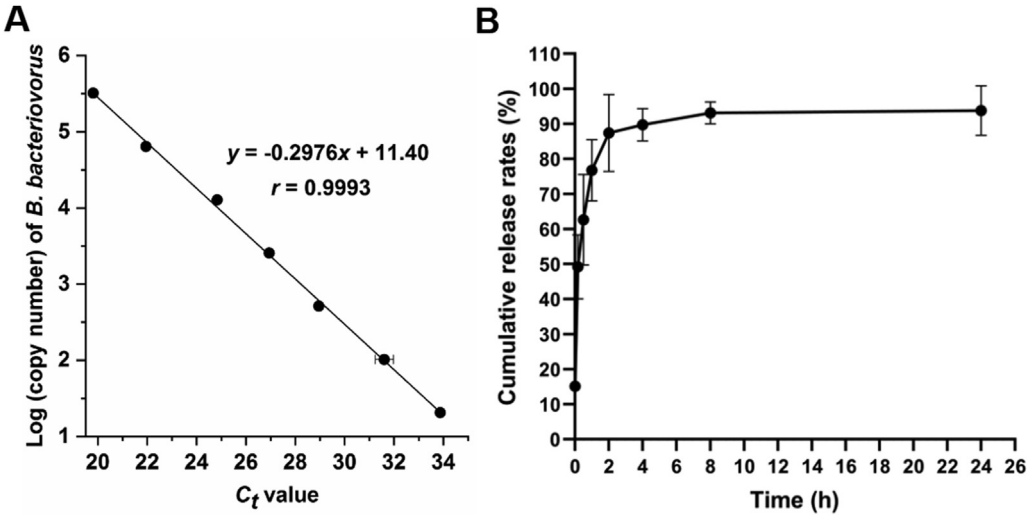

Figure 3 Quantitative detection of *B. bacteriovorus* release from BG *in vitro*. (A) Standard curve of *B. bacteriovorus* in solutions ranging from 10^1 to 10^6 copies per reaction. (B) Release profile of *B. bacteriovorus* from BG. Data are presented as mean ± SD ($n = 3$).

The large inhibition zone of *B. bacteriovorus* demonstrated that it killed distant bacteria by proliferation and self-propelling, harnessing the power of predatory bacteria as a "live antibiotic". Besides *V. vulnificus*, BG also exhibited strong antibacterial activity against *E. coli*, *P. aeruginosa*, meropenem-resistant *P. aeruginosa*, and their mixture (Supporting Information Fig. S3A−E). Moreover, we found that BG and meropenem had the similar antibacterial ability against *P. aeruginosa.* But only BG showed strong anti-resistant *P. aeruginosa* activity (Fig. S3F−G). Therefore, the broad-spectrum antibacterial ability and resistance-independent property of BG are confirmed. The survival time of *B. bacteriovorus* in BG was very long. After storage of BG at 4 °C for Days 0, 1, 3, 5, and 7, the antibacterial activity of *B. bacteriovorus* still maintained strong with the similar inhibition zone against *V. vulnificus* (Fig. 4D and E). However, after exposure in the air for 24 h, the antibacterial activity of BG had a little decrease (Supporting Information Fig. S4), which might be attributed to the water loss from the hydrogel and the motility decrease of *B. bacteriovorus.* Therefore, BG should be sealed in the package before use.

3.5. *High improved infected wound healing ability of BG*

The *V. vulnificus*-infected wounds were serious due to the infection, especially in the early stage (Fig. 5A). Although the infected control group had gradually accelerating wound closure, the healing speed was still less than that of the uninfected control group (Fig. 5A and B). Aquacel Ag showed the remarkable superiority of wound healing in the early stage (Day 3) compared with the infected control that secreted yellow exudates, but no significant difference from the uninfected control during the whole wound healing process (Fig. 5A and B). The rapid bacterial inhibition of Aquacel Ag could be the major reason, although the infection severity changed weak in the late stage and the bactericidal ability became not important. In contrast, BG showed accelerating wound healing compared to the other groups including the uninfected control with statistical significance ($P < 0.01$ or $P < 0.001$). On Day 10, the wound closure of the BG group had approached 100%, although those of the uninfected control group and the Aquacel Ag group approached 80%, and that of the infected control group was about 70%.

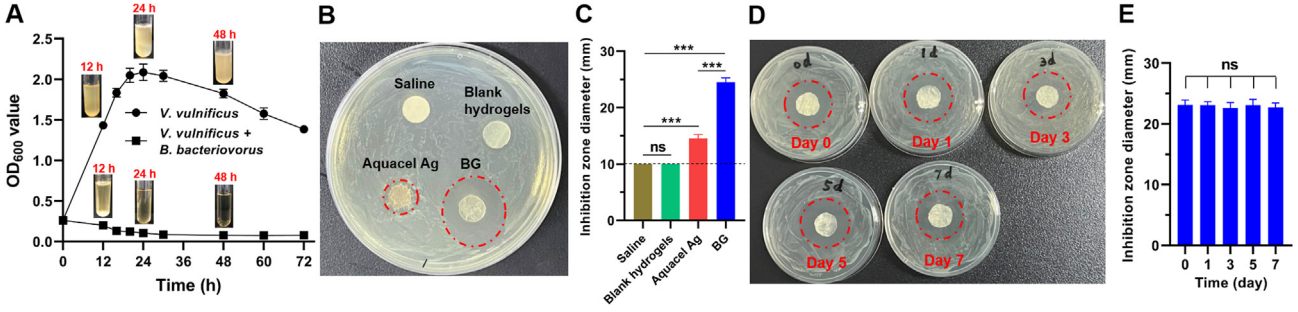

Figure 4 Bactericidal ability of BG. (A) OD_{600} values and typical appearance of *V. vulnificus* suspensions and the mixture suspensions of *B. bacteriovorus* and *V. vulnificus* depending on time. (B) Inhibition zone photographs of different samples against *V. vulnificus.* (C) Analysis of the inhibition zones in Graph B. (D) Inhibition zone photographs of BG stored at 4 °C for different days. (E) Analysis of the inhibition zones in Graph D. Data are presented as mean ± SD ($n = 3$, $^{***}P < 0.001$; ns, not significant).

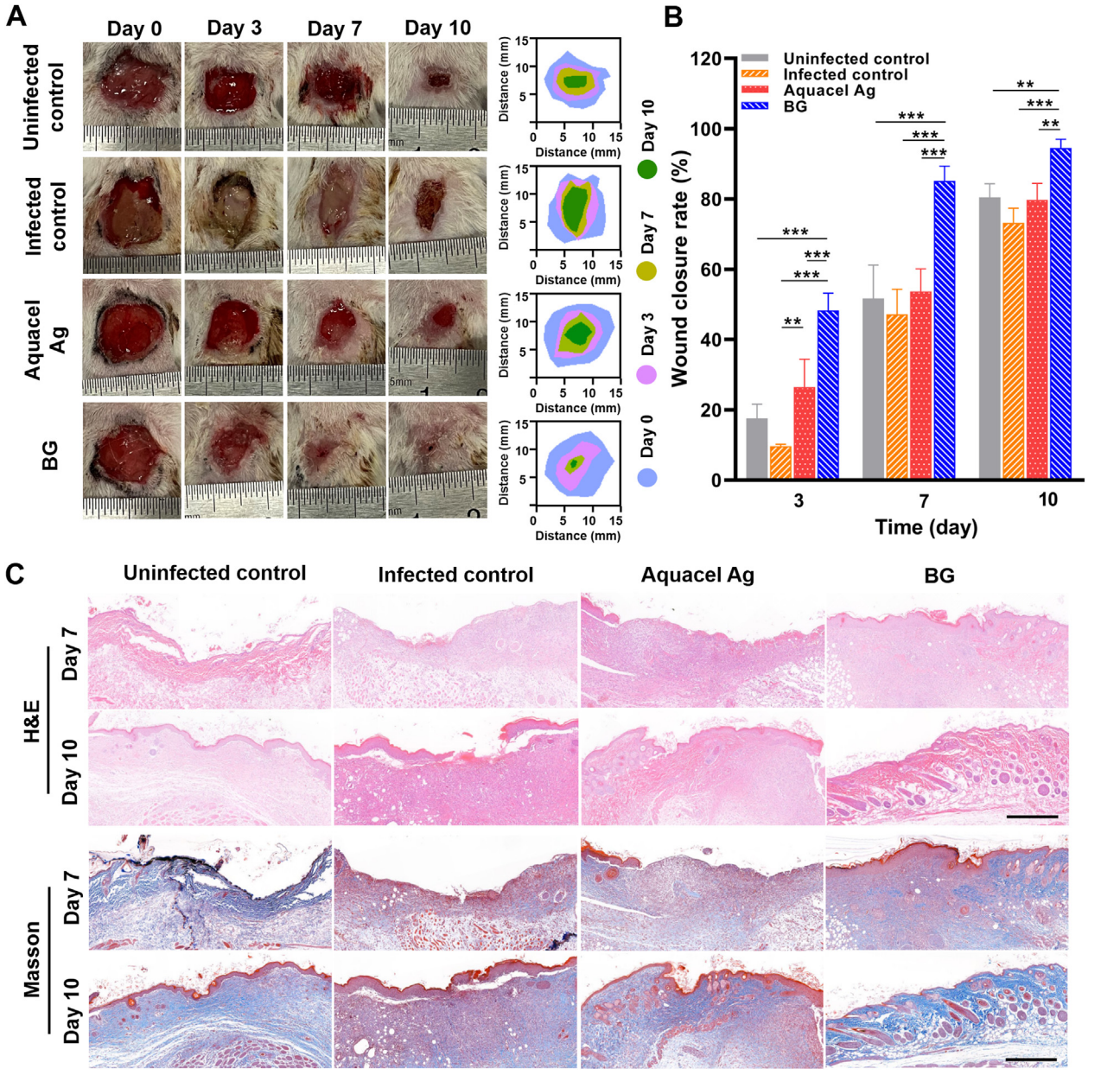

Figure 5 Wound healing ability of different preparations. (A) Photos and simulated area of the wounds on Days 0, 3, 7, and 10 in different groups. The minimal scale of the ruler is 0.5 mm. (B) Wound closure rates in different groups. (C) H&E staining and Masson's trichrome staining images of the wounds on Day 7 and 10 in different groups. Scale bar = 500 μm. Data are presented as mean ± SD ($n = 3$, $^{**}P < 0.01$, $^{***}P < 0.001$).

One key representation of wound healing is wound closure that prevents the further invasion of microorganisms[54]. Infected wounds usually have a slower healing process than uninfected wounds due to the severe impediment of bacterial infection[55]. If the infection was inhibited, the wounds would be healed quickly as the same as the uninfected wounds, *e.g.*, the Aquacel Ag group *vs.* the uninfected control group (Fig. 5B). Interestingly, BG can improve the healing of infected wounds much better than that of uninfected wounds, where the former had the wound closure rates of 48%, 85%, and 94% on Days 3, 7, and 10, respectively, and the latter had 18%, 52%, and 81%. The such good wound healing effect of BG must be related to not only its strong antibacterial ability but also the unique dual-network hydrogel structure of PVA/SA hydrogels. The next studies further uncovered the mechanism of BG enhancing the healing of infected wounds.

The pathological sections of the wounds showed the details of wound healing. On Day 7, local tissue necrosis, epidermal damage, and inflammatory cells aggregation occurred in all the groups except the BG group (Fig. 5C). The BG group showed a complete epithelial layer with only a little inflammatory cell infiltration. On the contrary, the infected control group and the Aquacel Ag group showed a large accumulation of inflammatory cells, indicating severe inflammation after bacterial infection. The uninfected control group showed wide gap between the epidermis and dermis in the wound. In the BG group, the granulation tissue was completely covered by the new layer of epidermis and the wound

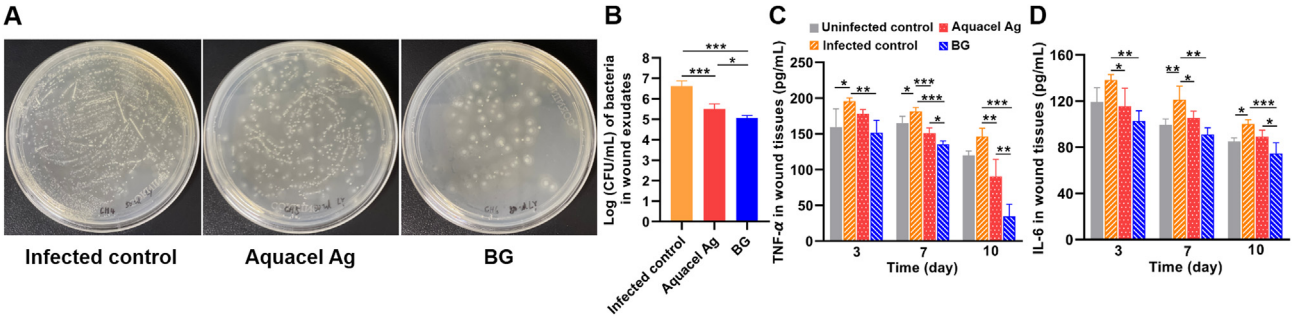

Figure 6 Bacterial numbers and pro-inflammatory cytokine levels in wounds. Photos of *V. vulnificus* colonies in wound exudates on Day 3 (A), and the colony counts (B). Expressions of TNF-α (C) and IL-6 (D) in wound tissues. Data are presented as mean ± SD ($n = 3$, $^{*}P < 0.05$, $^{**}P < 0.01$, $^{***}P < 0.001$).

space shrank without obvious necrosis. On Day 10, BG had improved the formation of continuous and intact epidermis and the granulation tissue was well formed and skin appendages such as sebaceous glands and hair follicles were emerging. In contrast, there were still inflammatory and necrotic cells in the infected control group and the Aquacel Ag group and the dermis was disorganized, indicating a slow wound healing process.

In addition, the Masson's trichrome staining of wound tissues further indicated the difference of collagen fiber formation and deposition between the groups (Fig. 5C). On Day 7, a large area of light blue collagen fibers appeared in the BG group, while the red-stained necrotic tissue with little blue-stained collagen appeared in the infected control group and the Aquacel Ag group. On Day 10, the BG group possessed uniform and order mature collagen deposition, similar to the normal structure of dermis. Whereas, the Aquacel Ag group exhibited the comparatively dense collagen formation to the BG group but the collagen fibers were disordered. Aquacel Ag could delay wound re-epithelialization due to its cytotoxic effect against rapidly proliferating cells such as fibroblasts and keratinocytes[50].

3.6. *High in vivo antibacterial and anti-inflammatory ability of BG*

The above experiment had shown the infection achieved the most on Day 3 (Fig. 5A). The wound exudates of different groups were collected and incubated on this day and we found that the infected control had a great deal of bacteria much more than the two treatment groups (Fig. 6A and B). Moreover, the number of bacteria in the BG group was much lower than that in the Aquacel Ag group. Therefore, BG exerted high *in vivo* antibacterial ability.

The pro-inflammatory cytokines including TNF-α and IL-6 are involved in the up-regulation of inflammatory reactions, which hinder wound healing[56]. TNF-α and IL-6 in the infected control group maintained the highest levels in the whole process among all the groups (Fig. 6C and D), indicating severe inflammatory responses after bacterial infection in the wounds. In contrast, the levels of TNF-α and IL-6 in the BG group always kept lowest, and significantly lower than those in the Aquacel Ag group on Days 7 and 10 ($P < 0.05$ or $P < 0.01$). Bacterial endotoxins promote the expression of pro-inflammatory cytokines (*e.g.*, TNF-α and IL-6).

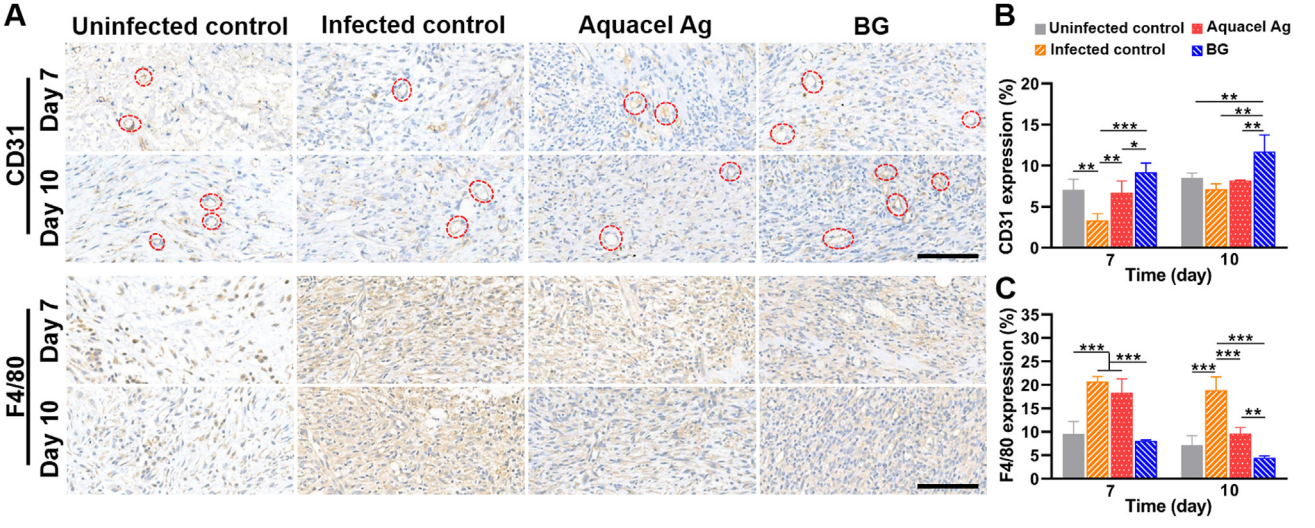

Figure 7 Expressions of CD31 and F4/80 in the wound tissues on Days 7 and 10. The images of immunohistochemical staining of CD31 and F4/80 (A). The quantitative analysis of CD31 (B), and F4/80 (C). Red circles indicate blood vessels. Scale bar = 100 μm. Data are presented as mean ± SD ($n = 6$, $^{*}P < 0.05$, $^{**}P < 0.01$, $^{***}P < 0.001$).

The high antibacterial ability of BG also led to weak inflammatory response, improving wound healing.

3.7. Enhanced expression of CD31 and reduced expression of F4/80 by BG

Neovascularization reflects the degree of tissue reconstruction and skin function recovery. The normal wound repair requires the formation of blood vessels in the new dermis to provide oxygen and nutrients. In general, angiogenesis involves the proliferation and migration of endothelial cells. Therefore, the expression of CD31, a biomarker of endothelial cells, is used to analyze the neovascularization at the wound sites and tested by immunohistochemistry[57]. The positively stained endothelial cells lined in a liner or a closed loop shape are recognized as a blood vessel[58]. On Day 7, the CD31 expression in the BG group was higher than those in the other groups, exhibiting the formation of more new blood vessels; on Day 10, the CD31 expression in the BG group was further enhanced with high significant differences from the other group (Fig. 7). Therefore, BG has the excellent wound healing effect *via* improving neovascularization.

F4/80 as a major macrophage marker indicates the maturation and activation of macrophages[59−61]. The massive proliferation and infiltration of macrophages are induced by wound infections and the activated macrophages could improve the production of excessive pro-inflammatory cytokines, leading to tissue injuries[62]. Brown-stained F4/80 expressions indicate the level of macrophages at the wound sites. On Days 7 and 10, the BG group always kept low F4/80 levels similar to the uninfected control group. However, on Day 7, both the infected control group and the Aquacel Ag group showed much higher F4/80 levels than the former two groups (Fig. 7C). On Day 10, the F4/80 levels in the Aquacel Ag group remarkably decreases, though higher than that in the BG group. Therefore, BG reduces macrophage activation and inflammatory response.

4. Conclusions

B. bacteriovorus is a promising biotherapy for various bacterial infections, although its growth and applications need an appropriate environment. However, *B. bacteriovorus* may be phagocytized by immune cells in the body so that its application in the immune cell-abundant deep tissues is limited. We created a hydrogel formulation to load *B. bacteriovorus*, providing the appropriate environment for its growth and expanding its topical application in treatment of wound infection. The high antibacterial ability of *B. bacteriovorus* and the improved wound healing function of hydrogels are organically combined; more importantly, the hydrogel is completely biocompatible. Based on the diversity of the preys of *B. bacteriovorus*, BG is a promising broad-spectrum treatment of infected wounds.

Acknowledgments

This work was partially supported by the National Natural Science Foundation of China (82073791).

Author contributions

Yan Liu and Yiguang Jin designed the research, carried out the experiments and performed data analysis. Bo Zhuang and Bochuan Yuan carried out part of the experiments and performed data analysis. Hui Zhang, Jingfei Li, Wanmei Wang and Ruiteng Li participated part of the experiments. Lina Du and Pingtian Ding directed part of the experiments. Yan Liu wrote the manuscript. Yiguang Jin revised the manuscript. All of the authors have read and approved the final manuscript.

Conflicts of interest

The authors declare no conflict of interest in this work.

Appendix A. Supporting information

Supporting data to this article can be found online at https://doi.org/10.1016/j.apsb.2022.05.005.

References

1. Elmahdi S, DaSilva LV, Parveen S. Antibiotic resistance of Vibrio parahaemolyticus and *Vibrio vulnificus* in various countries: a review. *Food Microbiol* 2016;**57**:128−34.
2. Hampton T. Novel programs and discoveries aim to combat antibiotic resistance. *JAMA* 2015;**313**:2411−3.
3. Baker-Austin C, Oliver JD. *Vibrio vulnificus*: new insights into a deadly opportunistic pathogen. *Environ Microbiol* 2018;**20**:423−30.
4. Baker-Austin C, Oliver JD. Vibrio vulnificus. *Trends Microbiol* 2020;**28**:81−2.
5. Fang Q, Yao Z, Feng L, Liu T, Wei S, Xu P, et al. Antibiotic-loaded chitosan-gelatin scaffolds for infected seawater immersion wound healing. *Int J Biol Macromol* 2020;**159**:1140−55.
6. Centers for Disease Control and Prevention (CDC). *Vibrio vulnificus & wounds*. 2019. Available from: https://www.cdc.gov/vibrio/wounds.html.
7. Leng F, Lin S, Wu W, Zhang J, Song J, Zhong M. Epidemiology, pathogenetic mechanism, clinical characteristics, and treatment of *Vibrio vulnificus* infection: a case report and literature review. *Eur J Clin Microbiol Infect Dis* 2019;**38**:1999−2004.
8. Baker-Austin C, Oliver JD, Alam M, Ali A, Waldor MK, Qadri F, et al. *Vibrio* spp. infections. *Nat Rev Dis Prim* 2018;**4**:8.
9. Wang X, Xu P, Yao Z, Fang Q, Feng L, Guo R, et al. Preparation of antimicrobial hyaluronic acid/quaternized chitosan hydrogels for the promotion of seawater-immersion wound healing. *Front Bioeng Biotechnol* 2019;**7**:360.
10. Pantanella F, Iebba V, Mura F, Dini L, Totino V, Neroni B, et al. Behaviour of *Bdellovibrio bacteriovorus* in the presence of gram-positive *Staphylococcus aureus*. *New Microbiol* 2018;**41**:145−52.
11. Caulton SG, Lovering AL. Bacterial invasion and killing by predatory *Bdellovibrio* primed by predator prey cell recognition and self protection. *Curr Opin Microbiol* 2020;**56**:74−80.
12. Dharani S, Kim DH, Shanks RMQ, Doi Y, Kadouri DE. Susceptibility of colistin-resistant pathogens to predatory bacteria. *Res Microbiol* 2018;**169**:52−5.
13. Willis AR, Moore C, Mazon-Moya M, Krokowski S, Lambert C, Till R, et al. Injections of predatory bacteria work alongside host immune cells to treat shigella infection in zebrafish larvae. *Curr Biol* 2016;**26**:3343−51.
14. Russo R, Kolesnikova I, Kim T, Gupta S, Pericleous A, Kadouri DE, et al. Susceptibility of virulent *Yersinia pestis* bacteria to predator bacteria in the lungs of mice. *Microorganisms* 2018;**7**:2.
15. Findlay JS, Flick-Smith HC, Keyser E, Cooper IA, Williamson ED, Oyston PCF. Predatory bacteria can protect SKH-1 mice from a lethal plague challenge. *Sci Rep* 2019;**9**:7225.
16. Atterbury RJ, Tyson J. Predatory bacteria as living antibiotics—where are we now?. *Microbiology* 2021;**167**:001025.

17. Atterbury RJ, Hobley L, Till R, Lambert C, Capeness MJ, Lerner TR, et al. Effects of orally administered *Bdellovibrio bacteriovorus* on the well-being and *Salmonella* colonization of young chicks. *Appl Environ Microbiol* 2011;**77**:5794−803.
18. Dwidar M, Monnappa AK, Mitchell RJ. The dual probiotic and antibiotic nature of *Bdellovibrio bacteriovorus*. *BMB Rep* 2012;**45**: 71−8.
19. Gupta S, Tang C, Tran M, Kadouri DE. Effect of predatory bacteria on human cell lines. *PLoS One* 2016;**11**:e0161242.
20. Shatzkes K, Tang C, Singleton E, Shukla S, Zuena M, Gupta S, et al. Effect of predatory bacteria on the gut bacterial microbiota in rats. *Sci Rep* 2017;**7**:43483.
21. Hori A, Watabe Y, Yamada M, Yajima Y, Utoh R, Seki M. One-step formation of microporous hydrogel sponges encapsulating living cells by utilizing bicontinuous dispersion of aqueous polymer solutions. *ACS Appl Bio Mater* 2019;**2**:2237−45.
22. Ming Z, Han L, Bao M, Zhu H, Qiang S, Xue S, et al. Living bacterial hydrogels for accelerated infected wound healing. *Adv Sci* 2021: e2102545.
23. Nagahama K, Kimura Y, Takemoto A. Living functional hydrogels generated by bioorthogonal cross-linking reactions of azide-modified cells with alkyne-modified polymers. *Nat Commun* 2018;**9**: 2195.
24. Lee JH. Injectable hydrogels delivering therapeutic agents for disease treatment and tissue engineering. *Biomater Res* 2018;**22**:27.
25. Yang Y, Liang Y, Chen J, Duan X, Guo B. Mussel-inspired adhesive antioxidant antibacterial hemostatic composite hydrogel wound dressing *via* photo-polymerization for infected skin wound healing. *Bioact Mater* 2022;**8**:341−54.
26. Liang Y, He J, Guo B. Functional hydrogels as wound dressing to enhance wound healing. *ACS Nano* 2021;**15**:12687−722.
27. Cheng H, Shi Z, Yue K, Huang X, Xu Y, Gao C, et al. Sprayable hydrogel dressing accelerates wound healing with combined reactive oxygen species-scavenging and antibacterial abilities. *Acta Biomater* 2021;**124**:219−32.
28. Cao J, Wang P, Liu Y, Zhu C, Fan D. Double crosslinked HLC-CCS hydrogel tissue engineering scaffold for skin wound healing. *Int J Biol Macromol* 2020;**155**:625−35.
29. Liang Y, Li Z, Huang Y, Yu R, Guo B. Dual-dynamic-bond cross-linked antibacterial adhesive hydrogel sealants with on-demand removability for post-wound-closure and infected wound healing. *ACS Nano* 2021;**15**:7078−93.
30. Huang Y, Zhao X, Zhang Z, Liang Y, Yin Z, Chen B, et al. Degradable gelatin-based IPN cryogel hemostat for rapidly stopping deep noncompressible hemorrhage and simultaneously improving wound healing. *Chem Mater* 2020;**32**:6595−610.
31. Li M, Liang Y, He J, Zhang H, Guo B. Two-pronged strategy of biomechanically active and biochemically multifunctional hydrogel wound dressing to accelerate wound closure and wound healing. *Chem Mater* 2020;**32**:9937−53.
32. Lee HR, Kim TH, Oh SH, Lee JH. Prednisolone-loaded coatable polyvinyl alcohol/alginate hydrogel for the treatment of atopic dermatitis. *J Biomater Sci Polym Ed* 2018;**29**:1612−24.
33. Morariu S, Bercea M, Gradinaru LM, Rosca I, Avadanei M. Versatile poly(vinyl alcohol)/clay physical hydrogels with tailorable structure as potential candidates for wound healing applications. *Mater Sci Eng C Mater Biol Appl* 2020;**109**:110395.
34. Zhuang B, Chen T, Xiao Z, Jin Y. Drug-loaded implantable surgical cavity-adaptive hydrogels for prevention of local tumor recurrence. *Int J Pharm* 2020;**577**:119048.
35. Gao L, Chen J, Feng W, Song Q, Huo J, Yu L, et al. A multifunctional shape-adaptive and biodegradable hydrogel with hemorrhage control and broad-spectrum antimicrobial activity for wound healing. *Biomater Sci* 2020;**8**:6930−45.
36. Boileau MJ, Mani R, Clinkenbeard KD. Lyophilization of *Bdellovibrio bacteriovorus* 109J for long-term storage. *Curr Protoc Microbiol* 2017;**45**:7b.3.1−15.
37. Ricciardi R, Gaillet C, De Rosa C, Lauprêtre F. Investigation of the crystallinity of freeze/thaw poly(vinyl alcohol) hydrogels by different techniques. *Macromolecules* 2004;**37**:9510−6.
38. Wang L, Shelton RM, Cooper PR, Lawson M, Triffitt JT, Barralet JE. Evaluation of sodium alginate for bone marrow cell tissue engineering. *Biomaterials* 2003;**24**:3475−81.
39. Lee CS, Gleghorn JP, Won Choi N, Cabodi M, Stroock AD, Bonassar LJ. Integration of layered chondrocyte-seeded alginate hydrogel scaffolds. *Biomaterials* 2007;**28**:2987−93.
40. Funami T, Fang Y, Noda S, Ishihara S, Nakauma M, Draget K, et al. Rheological properties of sodium alginate in an aqueous system during gelation in relation to supermolecular structures and Ca^{2+} binding. *Food Hydrocolloids* 2009;**23**:1746−55.
41. Nuttelman CR, Henry SM, Anseth KS. Synthesis and characterization of photocrosslinkable, degradable poly(vinyl alcohol)-based tissue engineering scaffolds. *Biomaterials* 2002;**23**:3617−26.
42. Dalisson B, Barralet J. Bioinorganics and wound healing. *Adv Healthc Mater* 2019;**8**:e1900764.
43. Negus D, Moore C, Baker M, Raghunathan D, Tyson J, Sockett RE. Predator versus pathogen: how does predatory *Bdellovibrio bacteriovorus* interface with the challenges of killing Gram-negative pathogens in a host setting?. *Annu Rev Microbiol* 2017;**71**:441−57.
44. Chen G, He L, Zhang P, Zhang J, Mei X, Wang D, et al. Encapsulation of green tea polyphenol nanospheres in PVA/alginate hydrogel for promoting wound healing of diabetic rats by regulating PI3K/AKT pathway. *Mater Sci Eng C Mater Biol Appl* 2020;**110**:110686.
45. Lai Y, Dong L, Zhou H, Yan B, Chen Y, Cai Y, et al. Coexposed nanoparticulate Ag alleviates the acute toxicity induced by ionic Ag^{+} *in vivo*. *Sci Total Environ* 2020;**723**:138050.
46. Luna-Vázquez-Gómez R, Arellano-García ME, García-Ramos JC, Radilla-Chávez P, Salas-Vargas DS, Casillas-Figueroa F, et al. Hemolysis of human erythrocytes by Argovit™ AgNPs from healthy and diabetic donors: an *in vitro* study. *Materials* 2021;**14**:2792.
47. Shatzkes K, Chae R, Tang C, Ramirez GC, Mukherjee S, Tsenova L, et al. Examining the safety of respiratory and intravenous inoculation of *Bdellovibrio bacteriovorus* and *Micavibrio aeruginosavorus* in a mouse model. *Sci Rep* 2015;**5**:12899.
48. Romanowski EG, Stella NA, Brothers KM, Yates KA, Funderburgh ML, Funderburgh JL, et al. Predatory bacteria are nontoxic to the rabbit ocular surface. *Sci Rep* 2016;**6**:30987.
49. Schwudke D, Linscheid M, Strauch E, Appel B, Zahringer U, Moll H, et al. The obligate predatory *Bdellovibrio bacteriovorus* possesses a neutral lipid A containing alpha-D-Mannoses that replace phosphate residues. *J Biol Chem* 2003;**278**:27502−12.
50. Burd A, Kwok CH, Hung SC, Chan HS, Gu H, Lam WK, et al. A comparative study of the cytotoxicity of silver-based dressings in monolayer cell, tissue explant, and animal models. *Wound Repair Regen* 2007;**15**:94−104.
51. Barnea Y, Weiss J, Gur E. A review of the applications of the hydrofiber dressing with silver (Aquacel Ag) in wound care. *Therapeut Clin Risk Manag* 2010;**6**:21−7.
52. Paddle-Ledinek JE, Nasa Z, Cleland HJ. Effect of different wound dressings on cell viability and proliferation. *Plast Reconstr Surg* 2006; **117**. 110S-20S.
53. Kadouri DE, To K, Shanks RM, Doi Y. Predatory bacteria: a potential ally against multidrug-resistant Gram-negative pathogens. *PLoS One* 2013;**8**:e63397.
54. Zhang X, Yao D, Zhao W, Zhang R, Yu B, Ma G, et al. Engineering platelet-rich plasma based dual-network hydrogel as a bioactive wound dressing with potential clinical translational value. *Adv Funct Mater* 2021;**31**:2009258.
55. Hou S, Liu Y, Feng F, Zhou J, Feng X, Fan Y. Polysaccharide-peptide cryogels for multidrug-resistant-bacteria infected wound healing and hemostasis. *Adv Healthc Mater* 2020;**9**:e1901041.
56. Liu W, Ou-Yang W, Zhang C, Wang Q, Pan X, Huang P, et al. Synthetic polymeric antibacterial hydrogel for methicillin-resistant *Staphylococcus aureus*-infected wound healing: nanoantimicrobial

self-assembly, drug- and cytokine-free strategy. *ACS Nano* 2020;**14**: 12905−17.
57. Mao X, Cheng R, Zhang H, Bae J, Cheng L, Zhang L, et al. Self-healing and injectable hydrogel for matching skin flap regeneration. *Adv Sci* 2019;**6**:1901124.
58. Wimmer RA, Leopoldi A, Aichinger M, Wick N, Hantusch B, Novatchkova M, et al. Human blood vessel organoids as a model of diabetic vasculopathy. *Nature* 2019;**565**:505−10.
59. Qian H, Bai Q, Yang X, Akakpo JY, Ji L, Yang L, et al. Dual roles of p62/SQSTM1 in the injury and recovery phases of acetaminophen-induced liver injury in mice. *Acta Pharm Sin B* 2021;**11**:3791−805.
60. Zhao J, Huang H, Zhao J, Xiong X, Zheng S, Wei X, et al. A hybrid bacterium with tumor-associated macrophage polarization for enhanced photothermal-immunotherapy. *Acta Pharm Sin B* 2022;**12**: 2683−94.
61. Lin HH, Stacey M, Stein-Streilein J, Gordon S. F4/80: the macrophage-specific adhesion-GPCR and its role in immunoregulation. *Adv Exp Med Biol* 2010;**706**:149−56.
62. Qiu H, Zhu S, Pang L, Ma J, Liu Y, Du L, et al. ICG-loaded photodynamic chitosan/polyvinyl alcohol composite nanofibers: anti-resistant bacterial effect and improved healing of infected wounds. *Int J Pharm* 2020;**588**:119797.